ISSN 1027-4510, Journal of Surface Investigation: X-ray, Synchrotron and Neutron Techniques, 2017, Vol. 11, No. 4, pp. 853–864. © Pleiades Publishing, Ltd., 2017.
Original Russian Text © Yu.A. Novikov, 2017, published in Poverkhnost', 2017, No. 8, pp. 73–86.

Monte Carlo Method in Scanning Electron Microscopy. 1. Modeling and Experiment

Yu. A. Novikov[a, b]

[a] *Prokhorov General Physics Institute, Russian Academy of Sciences, Moscow, 119991 Russia*
[b] *National Research Nuclear University MEPhI (Moscow Engineering Physics Institute), Moscow, 115409 Russia*
e-mail: nya@kapella.gpi.ru

Received November 1, 2016

Abstract—Results of modeling by the Monte Carlo method of signals from a scanning electron microscope examining rectangular grooves in silicon are compared with experimental results obtained for a scanning electron microscope operating in the secondary slow electron collection mode. The comparison is performed for the peaks of signals characterizing the primary electron beam near the walls of rectangular grooves: the widths and amplitudes of the peaks, the integral contributions of the peaks, and the positions of the peaks relative to the walls of the grooves. The parameters and their dependences on the primary electron energy are compared. All dependences are very different in terms of the parameters of the peaks and their dependence on the primary electron energy. This proves that the traditional representation of the Monte Carlo method does not work in scanning electron microscopy.

Keywords: Monte Carlo method, statistical modeling, scanning electron microscope, virtual scanning electron microscope, secondary slow electrons, image-formation mechanisms

DOI: 10.1134/S1027451017040243

INTRODUCTION

Scanning electron microscopy is widely used in various areas of science, engineering, and technology [1–4]. However, the widest application of scanning electron microscopy has been attained in microelectronics and nanoelectronics [4–6]. In [7, 8], it was shown that measuring the linear sizes of elements of microchips is an important stage of microchip technology, substantially reducing the costs of developing the technology and producing microchips.

For this purpose, in Russia, a system for a scanning electron microscope (SEM) was developed, which converts the sizes from the Primary length standard (meter) to the nanoscale and makes it possible to measure the linear sizes of elements of microchips up to 10 nm [9, 10].

To date, a method for measuring the linear sizes of microchip elements up to 30 nm with a SEM has been developed [11]. In order to justify the measurement of such small sizes and theoretically develop new methods for measurements, a virtual scanning electron microscope (VSEM) was created [12–16]. Virtual measuring devices, to which the VSEM belongs, can be created by two methods: imitation of the operation of a real device [13] or by the simulation of information obtained on a real device [17].

For a VSEM, the operation of a real SEM is imitated by statistical modeling known as the Monte Carlo method. This method was developed in the middle of the 20th century and has gained wide application due to the simplicity of implementation and the advent of high-performance personal computers. For more than half a century, an uncountable number of works concerning the Monte Carlo method have been published, including works describing its application to scanning electron microscopy. These works are represented most completely in review [18]. Here, we add some works [19–25] published both before and after this review and lacking in [18] for different reasons.

In [13], it was shown that a VSEM cannot be created by the Monte Carlo method (in [14–16], it was created on the basis of a simulator). However, the application of the Monte Carlo method to scanning electron microscopy continues to widen (see, e.g., [18–23]).

It should be noted that, for the first time, the disagreement of the results of modeling by the Monte Carlo method [24] with the results of experiments with a SEM was demonstrated in [25]. However, this work was published a long time ago in a journal that is hard to come by in Russian. In this context, it is necessary to consider in detail the possibilities of application of the Monte Carlo method to scanning electron microscopy, the advantages and drawbacks of the method, and modeling results and to compare these results with

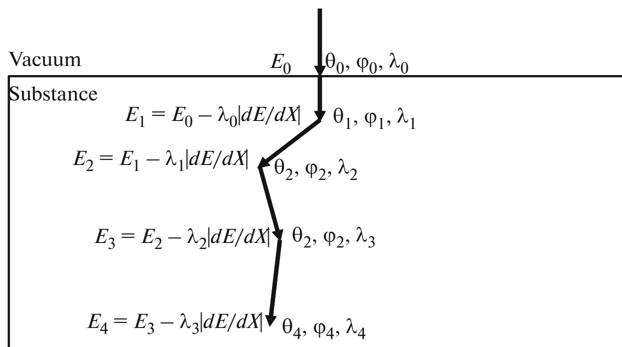

Fig. 1. Scheme of modeling of an electron trajectory in a substance by the Monte Carlo method.

real experiments with recent achievements in both modeling and experiment taken into account.

This work is the first part of an analysis of application of the Monte Carlo method to scanning electron microscopy. It is devoted to comparing the results of the modeling of rectangular relief structures with experiments conducted on a SEM with such structures.

1. MONTE CARLO METHOD

Application of the Monte Carlo method to scanning electron microscopy is based on imitation of the work of a real SEM: the interaction of beam electrons with the relief structure of a solid body. This interaction is described by the elastic scattering of electrons in the target substance and inelastic energy loss by primary electrons.

1.1. Description of the Method

The schematic of the Monte Carlo method imitating the operation of a SEM is shown in Fig. 1. The trajectory of a primary electron in a substance is represented by a broken line (the arrows indicate the direction of electron motion). At each kink point, the electron energy E_j at this point (j is the index of the kink in the trajectory ($j = 1, 2, 3, \ldots\ldots N$) and N is the number of kinks), the next free length λ_j, and the angles of inclination, θ_j and φ_j, of the next part of the trajectory relative to the current one are calculated by the following expressions [26]:

$$\lambda_j = \lambda \ln \gamma_k, \tag{1}$$

$$E_j = E_{j-1} - \lambda_j \left|dE/dX\right|, \tag{2}$$

$$\theta_j = \arccos\left(\frac{(1+2\beta)\gamma_{k+1} - \beta}{\beta + \gamma_{k+1}}\right), \tag{3}$$

$$\varphi_j = 2\pi\gamma_{k+2}, \tag{4}$$

where λ is the mean free length, β is the screening parameter for a scattering nucleus, γ_k is a current random number, and $k = 1, 2, 3, \ldots$ is the index of a random number.

The dynamics of the simulation is as follows. An electron with the initial energy E_0 enters the substance. In this case, the angles θ_0 and φ_0 of inclination of the electron trajectory in the substance are defined by the angle at which the electron enters the sample (for the perpendicular incidence, $\theta_0 = 0$ and $\varphi_0 = 0$). Using a random number generator and expression (1), the free length λ_0 is calculated and the electron energy E_1 at the end of the free length (the first kink in the trajectory) is determined by expression (2). In this case, the specific energy loss is usually calculated for the intermediate energy:

$$E = (E_j + E_{j-1})/2. \tag{5}$$

Taking into account the small difference between E_j and E_{j-1}, other variants are also possible.

Then the electron is displaced to a new kink point (Fig. 1), the new angles θ_1 and φ_1 are calculated by expressions (3) and (4), the new free length λ_1 by expression (1), etc. In each such case, a new random number is taken. This procedure is performed until satisfaction of all criteria for the modeling of the electron trajectory, which are specific to each author.

There are two types of modeling of the real beam size. In the first type, one or several trajectories are modeling for each coordinate of entry of an electron into the substance. The actual beam size in this case is obtained by summing the modeling trajectories of electrons incident into the entry zone bounded by the beam size. This variant of the method strongly reduces the modeling time, because the same trajectory is taken repeatedly for different beam positions. The drawback of this kind of modeling is the impossibility of modeling converging or diverging beams. In a number of cases, this circumstance greatly restricts the applicability of this method.

In the second variant, the beam position is fixed and trajectories in which the coordinates and entry angles vary according to the electron distribution in the beam and its convergence or divergence are modeling. Such modeling takes much more time, since, for the same beam position, one has to simulate many trajectories with different parameters. However, such modeling is more correct from the physical point of view and enables one to extend the applicability of the modeling due to the possibility to modeling inclined, converging, and diverging beams.

1.2. Elastic Electron Scattering

Elastic electron scattering used in the modeling is described by the electron mean free length λ (1) in a complex substance and is defined by the expression

$$\lambda = \left(N_A \rho \sum_i C_i \sigma_i / A_i \right)^{-1}, \qquad (6)$$

where N_A is the Avogadro number, ρ is the density of the substance, A_i is the atomic weight, C_i is the atomic concentration, and σ_i is the total elastic scattering cross section for atoms of the ith species.

The total elastic scattering cross section may have different forms. It is defined [24–26] by the expression describing electron scattering at a screened atomic nucleus:

$$\sigma_i = \frac{\pi e^4 Z_i (Z_i + 1)}{4E^2 \beta_i (\beta_i + 1)}, \qquad (7)$$

obtained by integrating the differential scattering cross section by the Rutherford formula with the screening effect taken into account. This formula reads

$$\frac{d\sigma_i}{d\Omega} = \frac{Z_i (Z_i + 1) e^4}{16E^2 \left(\sin^2 \theta/2 + \beta_i^2 \right)^2}, \qquad (8)$$

where e is the elementary charge, E is the electron energy, θ is the scattering angle, β_i is the parameter of screening, and Z_i is the atomic number of the chemical element of the ith species entering into the substance [24–26]. In this case, the parameter of screening is calculated by the expression

$$\beta_i = 5.43 Z_i^{2/3} / E, \qquad (9)$$

where the electron energy E is expressed in eV.

In the range of energies of 0.1–30 keV, currently used in scanning electron microscopy, the electron mean free path in silicon lies in the range of 0.25–56 nm. It should be noted that the distance between crystallographic planes in silicon is 0.3 nm. This means that formulas (7)–(9) cannot be used at electron energies below 100 eV.

1.3. Inelastic Energy Loss

The specific electron energy loss dE/dX is calculated in different works by different formulas. However, for high electron energies ($E > 1$ keV), the energy loss, as a rule [24–26], is calculated by the Bethe formula, describing the mean energy loss to the ionization of atoms in a complex substance:

$$\frac{dE}{dX} = -\frac{2\pi e^4 \rho N_A}{E} \sum_i \frac{C_i Z_i}{A_i} \ln \left(1.166 E / J_i \right), \qquad (10)$$

where e is the elementary charge, ρ is the density of the substance, E is the incident electron energy (in eV), N_A is the Avogadro number, A_i is the atomic weight, Z_i is the atomic number, C_i is the specific concentration, and J_i is the mean ionization potential (in eV) of atoms of the ith species, defined by the expression

$$J_i = 11.5 Z_i. \qquad (11)$$

The mean ionization potential for silicon is 161 eV. In the range of energies 0.1–30 keV, employed in scanning electron microscopy, the energy loss for silicon lies in the range of 25–1.6 eV/nm.

It is noted that, if the primary electron energy is lower than the mean ionization potential (11), formulas (10) and (11) cannot be used. Therefore, since expressions (7)–(9) for elastic scattering in silicon cannot be used for an electron energy below 100 eV, the criterion chosen in [23] for terminating modeling of the trajectory of a primary electron was the attainment of the mean ionization potential by the electron energy.

1.4. Random Number Generation

The main part in the Monte Carlo method is random number generation. However, random numbers do not exist in nature. A random number is a purely mathematical abstraction. A random number must have an infinite length. Any restriction on the length of a random number (for storage and utilization) converts a random number into a pseudorandom number. Therefore, one has to know, understand, and take into account the difference between random and pseudorandom numbers.

The main specific feature (and drawback) of pseudorandom numbers is their periodicity [13, 17]. The reason is that all pseudorandom number generators are generated by operations described by the expression

$$\gamma_{k+1} = \hat{P}(\gamma_k). \qquad (12)$$

The next pseudorandom number γ_{k+1} is obtained by some sequence of manipulations—the same for the given generator and all numbers and denoted by $\hat{P}$—with a current pseudorandom number γ_k. Since the length of a pseudorandom number is finite, there always exists a period after which the sequence of generated numbers repeats. Therefore, it is necessary to check for the periodicity of pseudorandom number generators employed for simulation. If the period of the generator is smaller than the amount of pseudorandom numbers required for modeling, the result of modeling acquires periodic distortions, which are impossible to detect and take into account.

In [15, 17], the pseudorandom number generator from the mathematical library of FORTRAN was

studied. This generator creates an array of numbers described well by the Gaussian distribution

$$g(\gamma) = \frac{I}{\sigma\sqrt{2\pi}} \exp\left(-\frac{(M-\gamma)^2}{2\sigma^2}\right), \qquad (13)$$

where $M = 0$ is the mean of the pseudorandom numbers, $\sigma = 1$ is the standard deviation, and $I = 10$ million is the number of generated numbers. The period of this generator is 30 million. This period is due not only to the method of pseudorandom-number generation but also by the fact that the numbers are stored and utilized in memory elements of a limited size (usually, 4 or 8 bytes). It should be noted that the period (3×10^7) of the generator is significantly smaller than the capacity of four-byte (4×10^9) and, moreover, eight-byte (18×10^{18}) number types.

Thus, the period of a pseudorandom-number generator is always significantly smaller than the capacity of the unit of memory used for the storage and utilization of pseudorandom numbers. This property of pseudorandom numbers should be taken into account when dealing with the Monte Carlo method. Thirty million pseudorandom numbers may be insufficient for modeling a particular process. For modeling by the Monte Carlo method of a 1000 × 1000-pix SEM image (the minimum image size employed nowadays) with 1000 trajectories at a point, with an electron energy of 30 keV, and silicon as the target substance requires at least 600 billion pseudorandom numbers [15]. Therefore, the image created with this generator will inevitably contain unknown periodic distortions. One can increase the period of the pseudorandom-number generator (e.g., by increasing the length of such numbers), but this leads to a dramatic (tens- and hundreds-fold) increase in the computation time, which is very undesirable.

In [13, 17], the time of generating an image with the aforementioned sizes on a personal computer with a Pentium Dual processor with a speed of 2.2 GHz, a motherboard-bus speed of 800 MHz, and control output to the screen of each tenth trajectory was calculated. Using these data, we find that the time for generating one image of 1000 lines with a continuously operating personal computer with such a processor will range from 7 days for $E = 1$ keV to 34 days for $E = 30$ keV. If all trajectories are output to the screen, the image generation time increases to a year and more. Thus, on a personal computer, one can obtain one or several signals rather than the entire image. For more detail, see [13].

The use of a supercomputer greatly reduces the modeling time. However, as was shown in [13], a supercomputer does not solve the given problem, because the Monte Carlo method usually takes into account only primary electron scattering. Although secondary electron scattering must be taken into account, it is almost impossible to do [13] due to the physics of the creation of secondary electrons and their scattering. The other reasons are the extremely high computation time and the absence of the necessary amount of pseudorandom numbers [13].

2. MODELING RESULTS

We might consider the modeling results presented in different works, but we will restrict the consideration to [24, 25], because the review of publications [18–23] showed an almost total lack of comparison between modeling by the Monte Carlo method and the experiment. Separate parts of the modeling were compared. For example, in [27], modeling and experimental backscattered electron spectra were compared and, in [28], modeling and experimental signals were compared. The sizes and shape of the experimental structure were recovered from the image of a cleavage of the structure. However, in [29], it was shown that measurements of the sizes from a cleavage give a large error. Therefore, the comparison in [28] was performed incorrectly. Comparison for all model parameters between the results of modeling by the Monte Carlo method [24] and the experiment was performed only in [25].

It should be noted that the results of the modeling of SEM signals by the Monte Carlo method, presented in [24], were obtained more than 20 years ago. The computer employed in that work had a much lower capacity than the aforementioned one. Therefore, in this work, we used various methods to reduce the computation time, which, as was shown later on more powerful computers, did not affect the modeling results.

Figure 2 shows images of the trajectories of primary electrons with an energy of 30 keV in silicon structures having grooves of a rectangular profile with a width of 0.5 μm and depths of 1.0 μm (Fig. 2a) and 2.0 μm (Fig. 2b), demonstrating the work of the modeling program. The program presented in [23] could modeling both normal and oblique incidence of the electron beam as well as convergence and divergence of the beam. Figure 2b shows the image of modeling trajectories of primary electrons near a rectangular groove in silicon under irradiation with a beam inclined by an angle of $\theta_0 = 30°$, a divergence–convergence angle of $\alpha = 10°$ (a large angle α was chosen for clarity), and a focal spot diameter of 30 nm.

As a result, signals for different energies of the electron beam were calculated (Fig. 3). For more detail of this modeling, see [24]. Analysis of these signal and signals obtained for other parameters was used in [25] for comparison with the experiment.

3. EXPERIMENTAL RESULTS

For comparison with the modeling by the Monte Carlo method, a series of experiments with relief rectangular structures (RRSs) in silicon were conducted

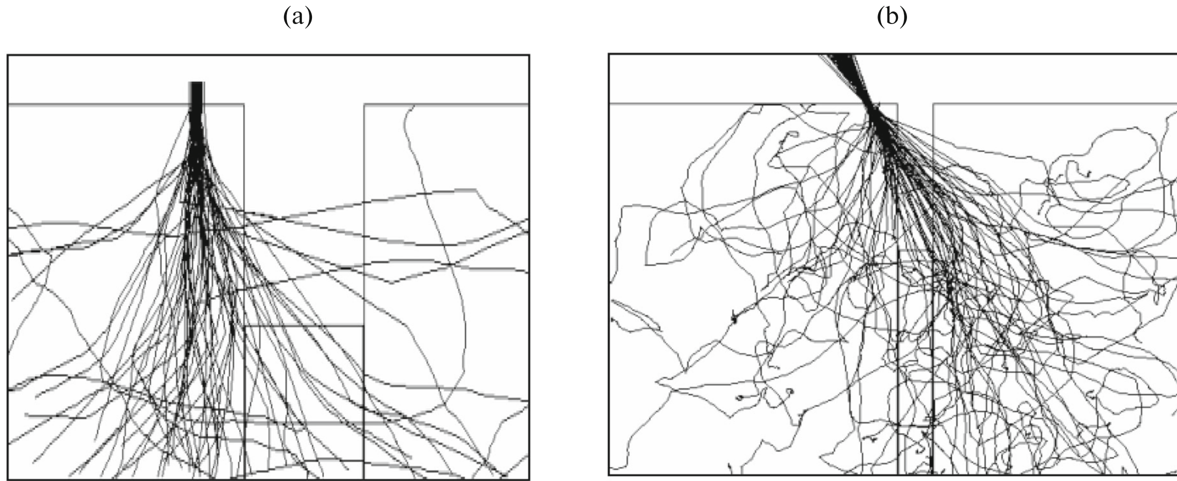

Fig. 2. Examples of electron trajectories near a groove in silicon with a width of 0.5 μm and depth of (a) 1.0 and (b) 2.0 μm for a beam diameter of 30 nm, electron energy of 30 keV, and (a) normal and (b) oblique incidence.

[30, 31]. Sets of four grooves on the surface of *n*-type (*n*-RRS) and *p*-type (*p*-RRS) silicon were created. The widths of the grooves in these sets are presented in Table 1. The widths were verified by the ellipsometry method [32, 33]. The grooves were produced with depths varying in the range of 0.1–12 μm, and the groove walls were parallel to an accuracy of 1 nm. However, in all experiments used for comparison with the modeling, the groove depths were 850 nm. For more detail on the technique of producing such structures, see [30, 31].

Figure 4 shows SEM images of grooves in *n*-RRS with a width of 150.7 and 434.7 nm (Fig. 4a and 4b, respectively), obtained using an S-4800 SEM in the secondary slow electron (SSE) collection mode, and Fig. 4c shows the SSE signals forming these images.

Figure 5 shows SEM images of grooves in *n*-RRS with a width of 150.7 nm (Fig. 5a) and 434.7 nm (Fig. 5b), obtained in the secondary slow electron collection (SSEC) mode using S-806 and SEM 515, respectively, and the signals forming these images. Comparing the signals in Figs. 4 and 5, we can conclude that the shape of the experimental signal is independent of the microscope using which the image is taken. It is also independent of the groove width.

The shape of the SSE signal [25, 30, 31] can be represented by the scheme shown in Fig. 6. In this scheme, control points *A*–*D* determining the shape of the signal are highlighted. Points *A* and *D* characterize the positions of the peaks of the signal, and point *B* and *C* characterize the positions of the boundaries of its bottom. Using these points, one can determine the characteristics of the signal: the distance L between peaks, the size G of the bottom, the peak amplitude I_a, the full width W at half-maximum, and the depth I_0 of the signal. This scheme also describes the shape of the model signal (Fig. 3).

4. COMPARISON BETWEEN MODEL AND EXPERIMENTAL RESULTS

SEM SSE signals are characterized by their peaks; therefore, the analysis of experimental signals and their comparison with the parameters of model signals (Fig. 6) were performed for the characteristics of the signal peaks: the full width at half maximum (FWHM; the height is measured from the zero level of the signal far from the groove); the amplitude; an integral quantity: the product of the FWHM by the amplitude; and the shift of the peaks relative to the groove walls.

4.1. Full Widths at Half-Maximum

The experiments are conducted using different electron microscopes with different magnifications, and modeling is performed using its own coordinate system. Therefore, to compare the model and experimental results, we pass to the coordinate system of the sample. In this case, the FWHM of the signal is determined by the reduced peak width:

$$w = mW = W/M, \quad (14)$$

where m is the pixel size in the image and M is the magnification of the microscope. In this case, the reduced width will be measured in nanometers.

Table 1. Groove width in *n*- and *p*-RRSs and their validation error

i	$l_i \pm \Delta l_i$, nm	
	n-RRS	*p*-RRS
1	92.8 ± 0.4	98.8 ± 0.4
2	128.5 ± 0.3	150.7 ± 0.3
3	344.4 ± 0.8	369.7 ± 0.8
4	486.2 ± 0.8	434.7 ± 0.8

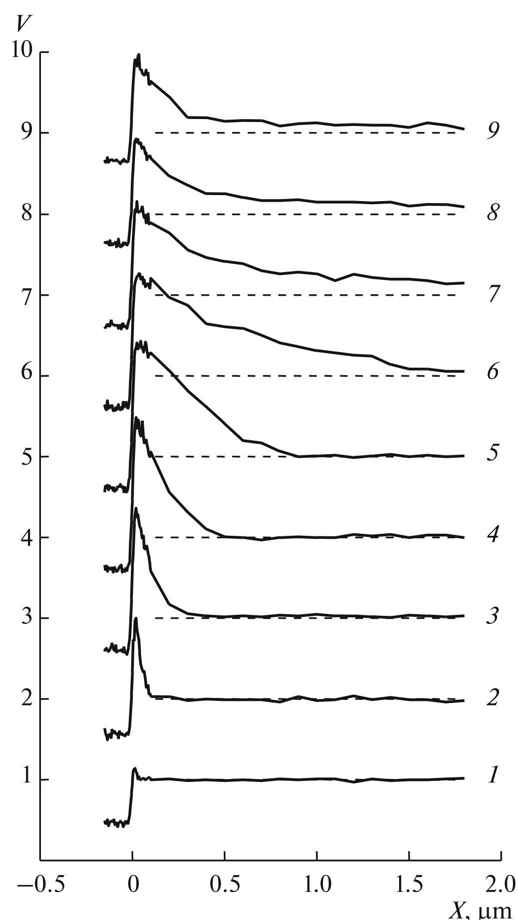

Fig. 3. Model signals obtained by the Monte Carlo method upon the scanning of a groove in silicon with a width of 0.5 μm and depth of 1.0 μm by an electron beam with a diameter of 30 nm and different primary electron energies for $\alpha = 0.2°$ and $\varphi = 0°$ [23]. Signals *1–9* correspond to $E = 1, 3, 5, 7, 10, 15, 20, 25$, and 30 keV. The zero abscissa value corresponds to the groove wall. The zero signal level is shown by horizontal dashed lines.

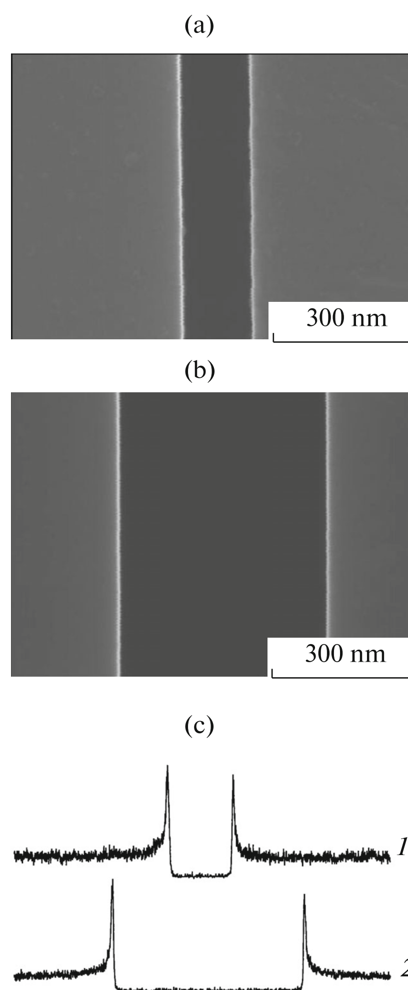

Fig. 4. Image of *n*-RRS grooves with a width of (a) 150.7 and (b) 434.7 nm and (c) the shapes of SSE signals from which these images consist: *1* and *2* signals.

Henceforth, the reduced width of a peak will be called the peak width.

At first, let us visually compare the model signal with a primary electron energy of 20 keV (signal *7* in Fig. 3) and experimental signals *1* and *2* in Fig. 4c. The peaks of the model signal have a width of 280 nm, whereas the experimental signals have a peak width of 10 nm. The peaks of the experimental signal are 28 times (!) narrower than the peaks of the model signal. Table 2 [30] presents the peak widths *w* of signals obtained using different SEMs with different beam radii *d*. These results show [30] that the peak width of the experimental signal is determined by half the beam diameter. The beam diameters in modern microscopes lie in the range of 10–50 nm and depend only on the SEM design and beam focusing.

Table 2. Peak widths *w* of SSE signals obtained on the scanning of RRSs by an electron beam with a diameter of *d* at primary electron energies of 20–25 keV

SEM	*w*, nm	*d*, nm
S-806	11.5 ± 0.3	29.1 ± 0.8
	25.8 ± 0.9	43.3 ± 1.7
SEM 515	20.3 ± 1.2	39 ± 7
	26.7 ± 1.7	57 ± 8
	16.9 ± 0.7	69 ± 8

At the same time, the peak width of the model signal is determined by the width of the region of multiple electron scattering (MES) in the target substance. This width depends on both the substance and the primary-electron energy but is practically independent of the beam diameter and SEM design.

This comparison is already sufficient to conclude that modeling by the Monte Carlo method in scanning electron microscopy does not give results consistent

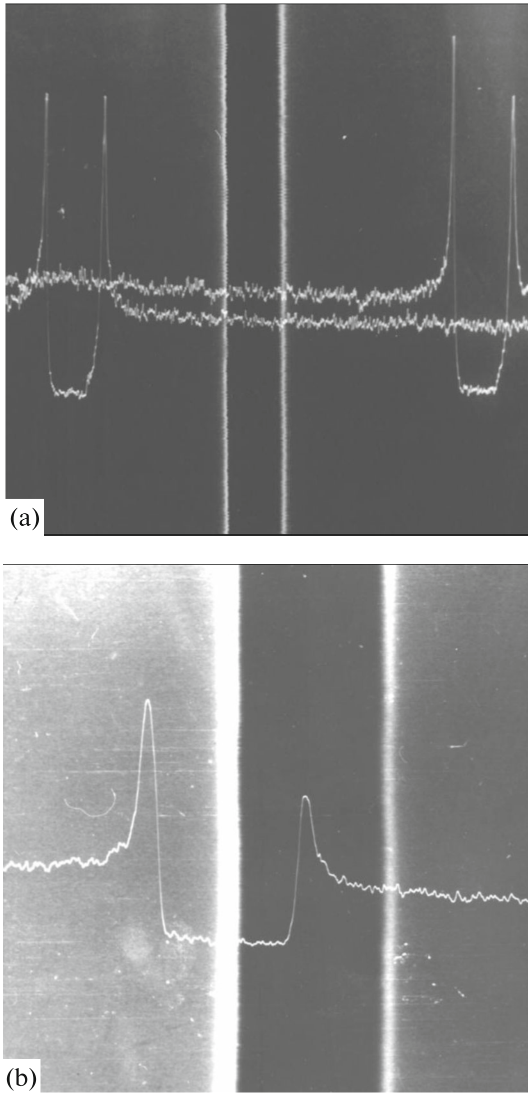

Fig. 5. Images of grooves and shapes of SSE signals from them obtained in the SSEC mode using different SEMs: (a) groove width of 150.7 nm, SEM S-806 and (b) groove width of 434.7 nm, SEM 515. For clarity, the signals are shifted with respect to its true position. The signals in image (a) correspond to different lines in the image.

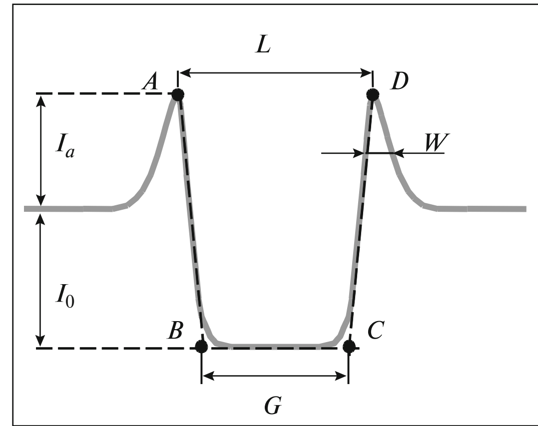

Fig. 6. Scheme of a SSE signal obtained upon the scanning of a rectangular groove by an electron beam with the axis parallel to the groove walls with control points and measured signal parameters.

with the experimental data. Let us continue the comparison.

The width of the MES region in a homogeneous substance can be estimated in terms of the mean electron transport length Λ [25, 26 , 34, 35]:

$$\Lambda = \frac{5.12\times10^{-4}E^2A}{\rho Z^2\ln\left(0.725E^{1/2}/Z^{1/3}\right)}, \quad (15)$$

where A is the atomic weight, Z is the atomic number, ρ is the density of the irradiated substance in g/cm^3, and E is the electron energy in eV. In this case, Λ is expressed in nanometers.

According to [25, 26 , 34, 35], an electron beam initially having the quadratic exponential distribution

$$f(x,y) = \frac{1}{\pi r^2}\exp\left(-\frac{x^2+y^2}{r^2}\right) \quad (16)$$

of the radius r and having passed through a film of a thickness p will also have a quadratic exponential distribution with a beam radius r_p defined as

$$r_p^2 = r^2 + \frac{4p^3}{3\Lambda}. \quad (17)$$

In [36, 37], a relationship was shown between the parameter r of a quadratic exponential beam and the effective beam diameter d

$$r = d/\sqrt{\pi}. \quad (18)$$

As a result, we obtain the beam diameter d_p after passing through a film with a thickness of p:

$$d_p^2 = d^2 + \frac{4\pi p^3}{3\Lambda}. \quad (19)$$

Thus, the quantity d_p characterizes the width of the MES region at the depth p.

The mean electron ranges in a substance is almost completely determined by the energy loss. Due to the complex character of electron motion, the mean electron ranges cannot be determined unambiguously. In [38], an empirical formula was obtained for the electron distribution over depth:

$$n(z) = \frac{mz^{m-1}}{z_0^m}\exp\left(-(z/z_0)^m\right), \quad (20)$$

where

$$z_0 = \frac{(40/\rho)E^{1.6}}{\Gamma\left((1/m)+1\right)}. \quad (21)$$

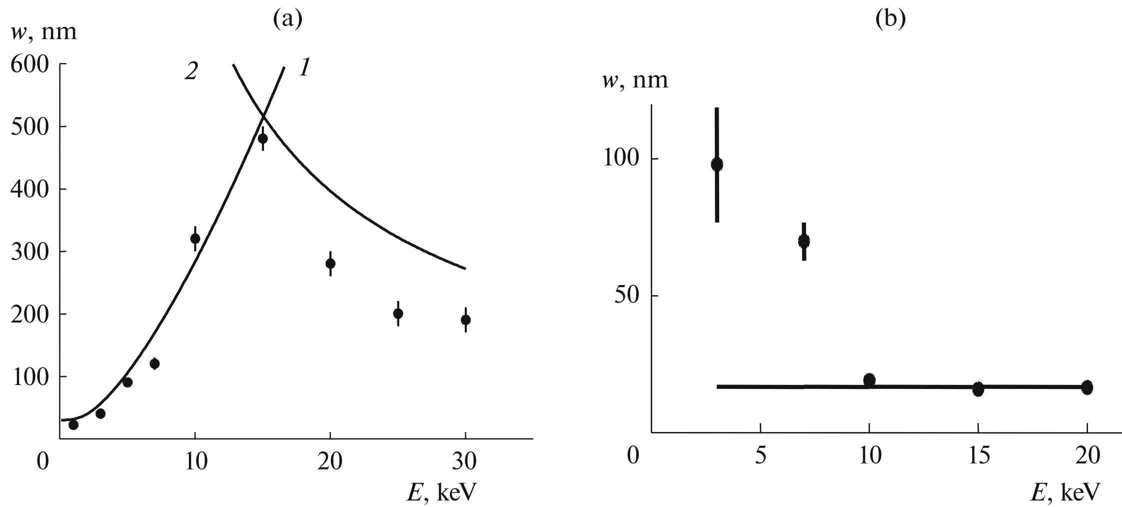

Fig. 7. Peak widths *w* of SSE signals (a) modeling by the Monte Carlo method and (b) experimental for different primary electron energies *E*.

Here, Γ is the gamma function, $m \sim 1.9$, ρ is the density of the substance (in g/cm^3), and E is the electron energy (in eV). In this case, z_0 is measured in nanometers.

Distribution (20) has a maximum at the depth z_m:

$$z_m = z_0\left(\frac{m-1}{m}\right)^{1/m}. \tag{22}$$

At the primary electron energy $E = 15$ keV in silicon, we have $z_m = 995$ nm, which agrees well with the groove depth $h = 1$ μm used in the modeling. This indicates the presence of two regions in the dependence of the peak width on the primary electron energy. In the first region ($E < 15$ keV), the groove depth is greater than the maximum z_m (22) of the electron distribution (20) over depth. In the second region ($E > 15$ keV), the groove depth h is smaller than z_m. Therefore, in the first region, the quantity p in formula (19) must be determined by z_m and, in the second region, by the groove depth h.

Let us compare the peak widths on the primary electron energy. Figure 7 shows these dependences for model (Fig. 7a) and experimental (Fig. 7b) signals. We see total disagreement not only between the peak widths but also between the dependences on the primary electron energy.

In the model dependence (Fig. 7a), with a decrease in the primary electron energy, the peak widths gradually increase and reach the maximum at an energy of 15 keV. With a further reduction in the energy, the peak widths of separate signals sharply decrease, approaching zero.

The model dependence (Fig. 7a) is divided into two energy regions, as shown above. At low energies (below 15 keV), the dependence

$$w = d_p \tag{23}$$

is described well by expression (19) under the condition $p = z_m/2$ (curve *1* in Fig. 7a). In the region of high energies (above 15 keV), dependence (23) is described sufficiently well (curve *2* in Fig. 7a) by expression (19) under the condition $p = h/2$.

Thus, the peak widths of model signals are determined by the part of the MES region that interacts with the groove. The dependence of the peak widths of the experimental signals (Fig. 7b) is also divided into two regions: below and above 10 keV. Above 10 keV, the peak widths of the experimental signals are very small (10–30 times smaller than those of the model signals) and are independent of the primary electron energy. This independence is represented by the horizontal line in Fig. 7b. Below 10 keV, the peak widths of the experimental signals sharply increase and become comparable with those of the model signals (Fig. 7a). Such behavior indicates [25] the existence of different mechanisms of image (signal) formation at different primary electron energies.

Thus, comparison between the peak widths of model and experimental signals has demonstrated that modeling by the Monte Carlo method is not applicable to scanning electron microscopy.

4.2. Peak Amplitudes of Signals

The amplitude analysis of SEM signals is almost never used. The reason is the use of the self-contrast mode for imaging, in which the parameters of the electron amplifier are unknown and can vary from

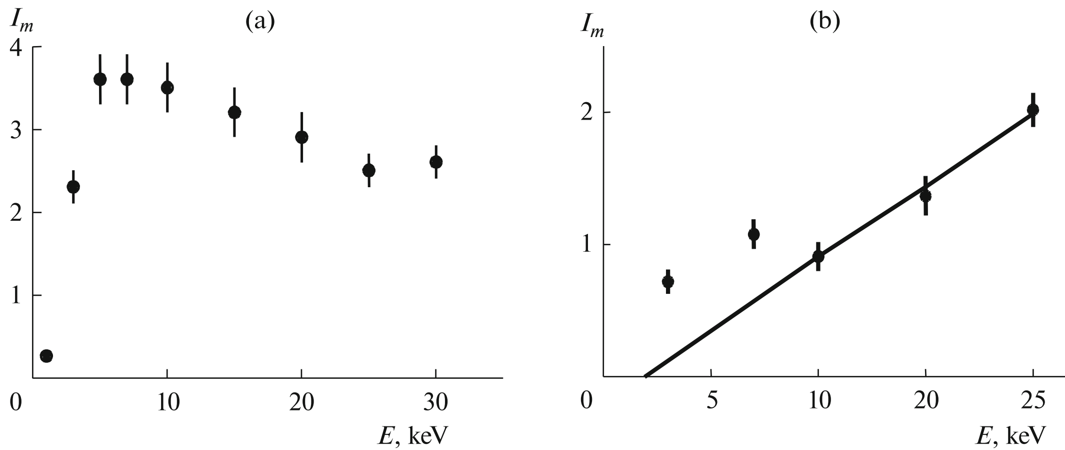

Fig. 8. Peak amplitudes I_m of (a) model and (b) experimental SSE signals vs. the primary electron energy *E*.

image to image. This difficulty can be overcome rather easily [39, 40].

The signal amplitude V at a specific image point is related to the amount v of emitted secondary electrons by a functional dependence represented by a Taylor series in powers of v:

$$V = \sum_{n=0}^{\infty} a_n v^n. \tag{24}$$

The electronic devices of a SEM operate in the linear mode. Then we impose on the expansion coefficients a_n the conditions $a_n = 0$ for $n \geq 2$. Thus, the signal V can be represented as

$$V = a_0 + a_1 v, \tag{25}$$

where a_0 is the drift of zero of the amplifier and a_1 is the gain factor. It should be noted that the values of a_0 and a_1 in modern scanning microscopes are never actually known. Therefore, amplitude analysis is usually not performed.

This difficulty can be removed [38, 39] if, in the experiment, we measure in a given image the difference between the signal amplitudes,

$$V_i - V_j = a_1(v_i - v_j), \tag{26}$$

and represent the results as the ratio of the differences:

$$\frac{V_i - V_j}{V_k - V_l} = \frac{v_i - v_j}{v_k - v_l}. \tag{27}$$

Thus, the representation of results in the form of the ratio of differences (27) makes them independent of the unknown parameters a_0 and a_1 and enables one to compare the data on (27) obtained by processing different images of the same structure on different SEMs.

The amplitude characteristics of signals can change in the process of measurements; therefore, they should be represented in form (27) if the peak amplitude I_a (Fig. 6) is defined as the distance on the ordinate axis between the signal levels at the peak and at the background, and the background amplitude I_0 is defined as the difference between the background and bottom levels (Fig. 6). Then, the quantity I_m (normalized peak amplitude) defined as

$$I_m = I_a / I_0, \tag{28}$$

will satisfy condition (27) and can be compared with both model and experimental values obtained on different images. Henceforth, the normalized peak amplitude of the signals will be called the peak amplitude.

Figure 8 shows the dependences of the peak amplitudes of model and experimental signals on the primary electron energy (we see different dependences). For model signals (Fig. 8a), with a decrease in the electron energy, the peak amplitude first slowly increases and then, at an energy of 5 keV, sharply decreases. At the same time, for experimental signals (Fig. 8b), the amplitude steadily (linearly) decreases as the primary electron energy decreases to 10 keV. The linearity is represented in Fig. 8b by a straight line. Below 10 keV, the peak amplitude of experimental signals is practically independent of the primary electron energy.

Thus, the comparison between the peak amplitudes of the model and experimental signals also shows that modeling by the Monte Carlo method is not applicable to scanning electron microscopy.

4.3. *Integral Characteristics of Signal Peaks*

The deviations between the characteristics of the peaks of model and experimental signals is probably related to a correlation between these characteristics (the peak widths and peak amplitudes of signals), since the presence of a correlation reduces its amplitude and leaves invariable the integral characteristics of the peaks. Therefore, a comparison between the integral characteristics of the peaks of model and experimental signals was performed. Such a character-

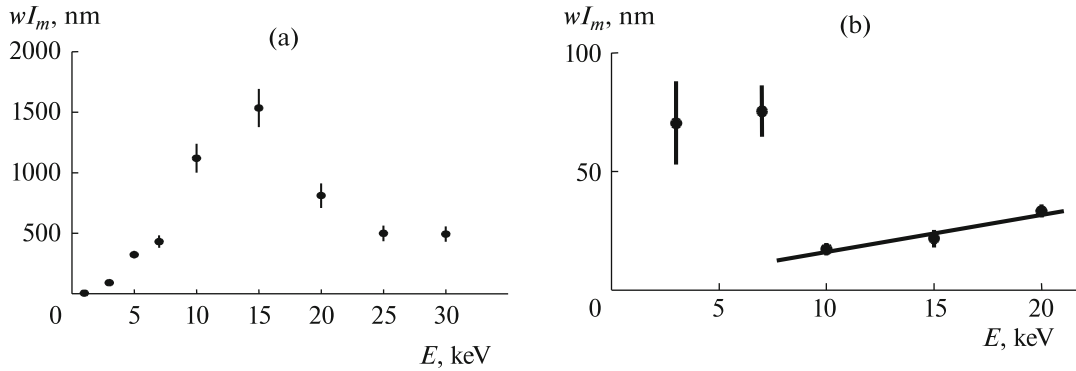

Fig. 9. Integral quantity wI_m of (a) model and (b) experimental SSE signals vs. the primary electron energy E.

istic was the product of the peak width w by the peak amplitude I_m, i.e., wI_m.

Figure 9 shows the dependences of the integral quantity wI_m on the primary electron energy for the model and experimental signals. We see that the integral quantity for the signal modeling by the Monte Carlo method exceeds tens of times that for experimental signals. Moreover, the dependences on the primary electron energy are also very different.

The modeling dependence (Fig. 9a) smoothly increases with a decrease in energy, attains a maximum at 15 keV, and then tends to zero. At the same time, the experimental dependence (Fig. 9b) linearly decreases. The linear dependence is represented in Fig. 9b by a straight line. Below an energy of 10 keV, the dependence on the energy sharply increases and remains constant within error. Such a dependence proves the absence of correlations between the peak width and peak amplitude but indicates the existence of different image-formation mechanisms [25] at different primary electron energies.

Thus, a comparison between the integral characteristics of model and experimental signals shows that the modeling by the Monte Carlo method is not applicable to scanning electron microscopy.

4.4. Signal Peak Positions

The signal peak positions will be determined with respect to the walls of a rectangular structure. The position of the wall is known in the modeling and unknown in the experiment. Therefore, we will use the relationship between the parameters L and G of the signal (Fig. 6), which relate the distance between peaks and the size of the signal bottom to the groove width l [30, 31]:

$$L = M(l + 2\delta) = (l + 2\delta)/m, \tag{29}$$

$$G = M(l - d) = (l - d)/m. \tag{30}$$

Here, δ is the shift of the signal peak with respect to the corresponding wall of a rectangular groove, d is the effective diameter of the SEM electron beam [35, 36] (henceforth, the beam diameter), M is the SEM magnification, and m is the pixel size in the image.

Using expressions (29) and (30), we can write two systems of equations:

$$\begin{cases} L_i = M(l_i + 2\delta) = (l_i + 2\delta)/m \\ L_j = M(l_j + 2\delta) = (l_j + 2\delta)/m \end{cases}, \tag{31}$$

$$\begin{cases} G_i = M(l_i - d) = (l_i - d)/m \\ G_j = M(l_j - d) = (l_j - d)/m \end{cases}, \tag{32}$$

where $i, j = 1, 2, 3, 4$; $i \neq j$. Solving this system, we obtain

$$\delta_{ij} = \frac{1}{2}\frac{G_j l_i - G_i l_j}{G_i - G_j}, \tag{33}$$

$$d_{ij} = \frac{G_i l_j - G_j l_i}{G_i - G_j}, \tag{34}$$

$$m_L = \frac{l_i - l_j}{L_i - L_j} = \frac{1}{M_L}, \quad m_G = \frac{l_i - l_j}{G_i - G_j} = \frac{1}{M_G}, \tag{35}$$

Here, M_L and m_L are parameters of the SEM and the image, determined using the distances between the peaks, and M_G and m_G are the parameters determined from the size of the signal bottom. The sets of rectangular structures (Table 1) have four grooves with different widths; therefore, one can not only determine d and δ but also establish that these parameters are independent of the groove width. For more details, see [25, 30, 31].

If $M_L = M_G$ and, correspondingly, $m_L = m_G$, and, if the beam diameters determined from different groove widths (34) coincide, then the mean values of δ_{ij} obtained by expression (33) will give the shift δ of the peak with respect to the edge of the groove.

Figure 10 shows the shift δ of the peaks of the model (Fig. 10a) and experimental (Fig. 10b) signals as a function of the primary electron energy. Again we observe significant deviations between the depen-

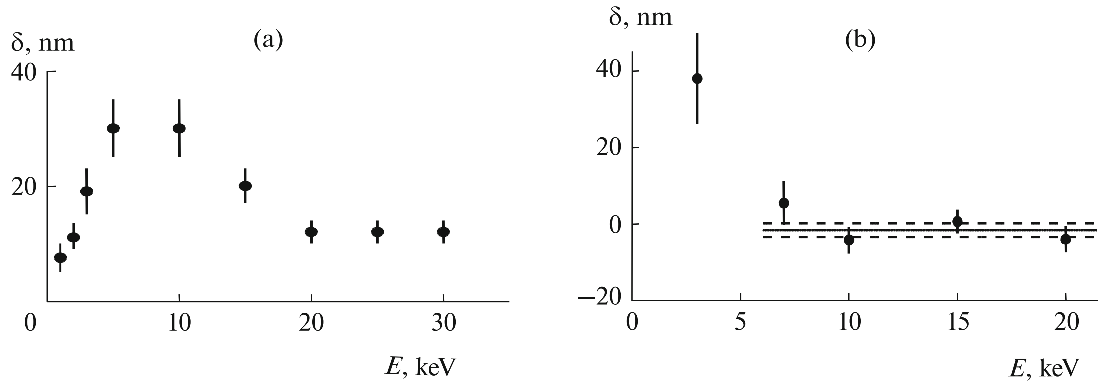

Fig. 10. (a) Model and (b) experimental shifts of the peaks of SSE signals for different primary electron energies E. The straight line in (b) corresponds to the mean value of δ in the range of energies above 10 keV. Dashed lines show the error range.

dences of the shift on the primary electron energy in absolute value and even sign. For the model signals, we always have $\delta > 0$ (the peak positions lie beyond the groove) and, for experimental signals, all variants: $\delta > 0$, $\delta < 0$, and $\delta = 0$ (the peak positions lie beyond the groove, inside the groove, and can coincide with the groove walls, respectively) are possible. Table 3 [25] presents the values of δ obtained for a long time in different experiments on different microscopes, which confirm the above assertion. It turned out [25, 39, 40] that the sign of δ is determined by beam focusing in the SEM. If the groove is scanned with a converging part of the beam, then $\delta > 0$; if it is scanned with a diverging part of the beam, then $\delta < 0$; and, if the groove is scanned with a focused part of the beam, then $\delta = 0$.

Table 3. Value of parameter δ obtained on S-806 and SEM 515 microscopes over 3 years

SEM	Type of RRS	$\delta \pm \Delta\delta$, nm
S-806	*p*	−5.9 ± 1.1
		−2.8 ± 0.4
		−3.8 ± 0.7
		1.6 ± 0.9
		0 ± 4
		−4 ± 4
	n	−0.3 ± 1.1
		−0.4 ± 0.3
		−0.1 ± 0.4
		1.1 ± 1.7
		3.8 ± 0.8
		5 ± 3
SEM 515	*p*	−1.5 ± 1.8
		−3.5 ± 2.3
		−4 ± 4
		−9 ± 4
		0 ± 3

Although the experimental value of δ can have an arbitrary sign and its absolute value can be zero, the sign and the absolute value of δ are retained in the range of primary electron energies above 10 keV. At energies below 10 keV, δ becomes positive and comparable with the model value.

There are no values of the beam parameters (convergence, divergence, parallelism of electron motion, the angle of incidence) at which the modeling of signals by the Monte Carlo method gives negative or zero values of δ. It is for this comparison that the modeling of the converging and diverging beam electrons presented in [24] was required.

Thus, the signal peak positions are not obtained by modeling by the Monte Carlo method.

CONCLUSIONS

The results of modeling by the Monte Carlo method of SEM signals obtained in the SSEC mode on scanning of rectangular grooves in silicon were compared with the experimental results obtained using a SEM with similar structures. It has been shown that all characteristics of the peaks of the model and experimental signals significantly differ in terms of the values of these characteristics and in their dependences on the primary electron energy. This proves that the traditional representation of the Monte Carlo method does not work in scanning electron microscopy.

In the next paper of this cycle, we will consider the reasons for the disagreement of the Monte Carlo method with the experiment and possibilities of correcting this method.

ACKNOWLEDGMENTS

I am grateful to A.V. Rakov and M.N. Filippov for participation in the experiments and useful discussions.

REFERENCES

1. J. I. Goldstein, D. E. Newbury, P. Echlin, D. C. Joy, C. Fiori, and E. Lifshin, *Scanning Electron Microscopy and X-Ray Microanalysis. A Text for Biologists, Materials Scientists, and Geologists* (Plenum Press, New York, London, 1981).
2. L. Reimer, *Scanning Electron Microscopy: Physics of Image Formation and Microanalysis* (Springer, Berlin, Heidelberg, New York, 1998).
3. *Scanning Microscopy for Nanotechnology. Techniques and Applications,* Ed. by W. Zhou and Z. L. Wang (Springer Science+Business Media, New York, 2006).
4. International Technology Roadmap for Semiconductors, 2013 Edition, Metrology (2013).
5. Yu. A. Novikov and A. V. Rakov, Meas. Tech. **42** (1), 20–26 (1999).
6. M. T. Postek and A. E. Vladar, *Critical Dimension Metrology and the Scanning Electron Microscope, Handbook of Silicon Semiconductor Metrology,* Ed. by A. C. Diebold (Marcel Dekker, New York, Basel, 2001), pp. 295–333.
7. M. T. Postek, Proc. SPIE **4608**, 84–96 (2002).
8. M. Postek, Vestn. Tekh. Regul., No. 7, 8–17 (2007).
9. V. Gavrilenko, Yu. Novikov, A. Rakov, and P. Todua, Nanoindustriya, No. 4, 36–42 (2009).
10. V. P. Gavrilenko, Yu. A. Novikov, A. V. Rakov, and P. A. Todua, Proc. SPIE **7405**, 740504-1–740504-8 (2009). doi 10.1117/12.826164
11. V. P. Gavrilenko, V. A. Kalnov, Yu. A. Novikov, A. A. Orlikovsky, A. V. Rakov, P. A. Todua, K. A. Valiev, and E. N. Zhikharev, Proc. SPIE **7272**, 727227-1–727227-9 (2009). doi 10.1117/12.814062
12. Yu. A. Novikov, J. Surf. Invest.: X-ray, Synchrotron Neutron Tech. **8** (6), 1244–1251 (2014). doi 10.1134/S1027451014060123
13. Yu. A. Novikov, J. Surf. Invest.: X-ray, Synchrotron Neutron Tech. **9** (3), 604–611 (2015). doi 10.1134/S1027451015030325
14. Yu. A. Novikov, Russ. Microelectron. **43** (4), 258–269 (2014). doi 10.1134/S1063739714040076
15. Yu. A. Novikov, Russ. Microelectron. **43** (6), 427–437 (2014). doi 10.1134/S1063739714060079
16. Yu. A. Novikov, Russ. Microelectron. **44** (4), 269–282 (2015). doi 10.1134/S1063739715030075
17. Yu. A. Novikov, J. Surf. Invest.: X-ray, Synchrotron Neutron Tech. **10** (1), 68–75 (2016). doi 10.1134/S1027451015060166
18. Y. G. Li, S. F. Mao, and Z. J. Ding, in *Applications of Monte Carlo Method in Science and Engineering,* Ed. by S. Mordechai (InTech, 2011), pp. 232–296.
19. V. Stary, in *Applications of Monte Carlo Method in Science and Engineering,* Ed. by S. Mordechai (InTech, 2011), pp. 195–230.
20. P. Zhang, H. Y. Wang, Y. G. Li, S. F. Mao, and Z. J. Ding, Scanning **34**, 145–150 (2012). doi 10.1002/sca.20288
21. Y. G. Li, P. Zhang, and Z. J. Ding, Scanning **35**, 127–139 (2013). doi 10.1002/sca.21042
22. Z. Ruan, M. Zhang, R. G. Zeng, Y. Ming, B. Da, S. F. Mao, and Z. J. Ding, Surf. Interface Anal. **46**, 1296–1300 (2014). doi 10.1002/sia.5565
23. J. S. Villarrubia, A. E. Vladar, B. Ming, R. J. Kline, D. F. Sunday, J. S. Chawla, and S. List, Ultramicroscopy **154**, 15–28 (2015).
24. Yu. A. Novikov, Phys., Chem., Mech. Surf. **11** (10), 1077–1084 (1995).
25. Yu. A. Novikov and A. V. Rakov, "Secondary electron emission from a relief surface of solids", *Mechanisms of secondary electron emission from a relief surface of solids*, Moscow: Nauka. Fizmatlit, 1998, pp. 3–99; (Proc. IOFAN, Vol. 55). [in Russian].
26. K. A. Valiev, *The Physics of Submicron Lithography* (Plenum Press, New York, 1992).
27. M. Dapor, E. I. Rau, and R. A. Sennov, J. Appl. Phys. **102**, 063705-1–063705-5 (2007).
28. M. Kadowaki, A. Hamaguchi, H. Abe, Y. Yamazaki, S. Borisov, A. Ivanchikov, and S. Babin, Proc. SPIE **7272**, 72723I-1–72723I-9 (2009).
29. Ch. P. Volk, Yu. A. Novikov, Yu. V. Ozerin, and A. V. Rakov, Meas. Tech. **44** (4), 365–369 (2001). doi 10.1023/A:1010911613346
30. Yu. A. Novikov, S. V. Peshekhonov, and I. B. Strizhkov, "The slit-like reference gauge structure for the SEM calibration and measurements of relief elements in submicron and nanometer ranges", Problems of linear measurements of microobjects in nanometer and submicron ranges. Moscow: Nauka, 1995, pp. 20–40; (Proc. IOFAN, Vol. 49). [in Russian].
31. Yu. A. Novikov, V. P. Gavrilenko, A. V. Rakov, and P. A. Todua, Proc. SPIE **7042**, 704208-1–704208-12 (2008). doi 10.1117/12.794834
32. Yu. A. Novikov and S. V. Peshekhonov, "The ellipsometry method errors of evaluation of a silicon and dioxide silicon film optical characteristics", *Problems of linear measurements of microobjects in nanometer and submicron ranges*, Moscow: Nauka, 1995, pp. 107–118; (Proc. IOFAN, Vol. 49). [in Russian].
33. V. P. Gavrilenko, Yu. A. Novikov, A. V. Rakov, and P. A. Todua, Proc. SPIE **7718**, 77181B-1–77181B-10 (2010). doi 10.1117/12.853898
34. R. W. Nosker, J. Appl. Phys. **40**, 1872–1882 (1969).
35. I. Brodie and J. J. Muray, *The Physics and Microfabrication* (Plenum Press, New York, London, 1982).
36. Ch. P. Volk, E. S. Gornev, Yu. A. Novikov, Yu. I. Plotnikov, A. V. Rakov, P. A. Todua, Yu. A. Novikov and S. V. Peshekhonov, "Problems of measurement of geometric characteristics of electron probe of scanning electron microscope", *Linear measurements in micrometer and nanometer ranges for microelectronics and nanotechnology.* Moscow: Nauka, 2006, pp. 77–120; (Proc. IOFAN, Vol. 62) [in Russian].
37. V. P. Gavrilenko, Yu. A. Novikov, A. V. Rakov, and P. A. Todua, Proc. SPIE **7042**, 70420C-1–70420C-12 (2008). doi 10.1117/12.794891
38. A. F. Makhov, Fiz. Tverd. Tela **2** (9), 2172–2175 (1960).
39. Yu. A. Novikov, A. V. Rakov, and I. Yu. Stekolin, *Physics, Chemistry, and Mechanics of Surfaces* **10** (4), 501–511 (1995).
40. Yu. A. Novikov and A. V. Rakov, Surf. Invest. **15** (8), 1177–1194 (2000).

Translated by E. Chernokozhin